nature COMMUNICATIONS

ARTICLE

Received 29 Jan 2013 | Accepted 8 May 2013 | Published 13 Jun 2013

DOI: 10.1038/ncomms2993

Synthetic regimes due to packing constraints in dendritic molecules confirmed by labelling experiments

Baozhong Zhang[1], Hao Yu[1], A Dieter Schlüter[1], Avraham Halperin[2] & Martin Kröger[3]

Classical theory predicts that branching defects are unavoidable in large dendritic molecules when steric congestion is important. Here we report first experimental evidence of this effect via labelling measurements of an extended homologous series of generations $g = 1 \ldots 6$ of dendronized polymers. This system exhibits a single type of defect interrogated specifically by the Sanger reagent thus permitting to identify the predicted upturn in the number of branching defects when g approaches g_{max} and the polymer density approaches close packing. The average number of junctions and defects for each member of the series is recursively obtained from the measured molar concentrations of bound labels and the mass concentrations of the dendritic molecules. The number of defects increases at $g = 5$ and becomes significant at $g = 6$ for dendronized polymers where the g_{max} was estimated to occur at $6.1 \leq g_{max} \leq 7.1$. The combination of labelling measurements with the novel theoretical analysis affords a method for characterizing high g dendritic systems.

[1] Laboratory of Polymer Chemistry, Department of Materials, ETH Zurich, Wolfgang-Pauli-Strasse 10, HCI J 541, CH-8093 Zurich, Switzerland. [2] Université Grenoble 1/CNRS, LIPhy UMR 5588, 38041 Grenoble, France. [3] Polymer Physics, Department of Materials, ETH Zurich, Wolfgang-Pauli-Strasse 10, HCI J 541, CH-8093 Zurich, Switzerland. Correspondence and requests for materials should be addressed to A.H. (email: avraham.halperin@ujf-grenoble.fr).

Intense research efforts are devoted to dendritic molecules comprising of repeatedly branched chains known as dendrons. The dendrons can be attached to point-like cores, to linear polymer chains or to surfaces thus giving rise to three leading structural families of dendritic molecules: dendrimers[1–5], dendronized polymers (DP)[6–9] and forests[10–12]. Their masses and spans depend on their generation g specifying the number of branching sites along a path between the attachment site and the terminus. The synthesis of ideal dendritic molecules with perfectly regular branching is conceivable for low g values. However, packing constraints rule out such perfect structures at high g when branching defects are unavoidable. The crossover between the two regimes occurs at a theoretically well-defined g_{max}[10,12–15] discussed below. Since the first reports of well-characterized dendrimers in 1985 (refs 16–19), thousands of research articles addressed their synthesis, properties and applications[1–9, 20–23]. Recent activity in this area reflects a growing interest in biomedical applications such as bio-imaging, gene and drug delivery[24–28]. The overwhelming majority of the literature concerns the $g \ll g_{max}$ range and highlights structural perfection. In marked distinction, this work focuses on the vicinity of g_{max}, the associated onset of structural imperfection and its characterization. It reports first direct evidence for g_{max} and the associated branching defects. It is enabled by synthesis of a homologous series of DP approaching the vicinity of g_{max}, their characterization and a theoretical framework for quantifying the number of defects. g_{max} of a DP occurs at relatively low values thus rendering the synthesis feasible. The near g_{max} range merits attention for two reasons. First, the existence of the two synthetic regimes is a qualitative signature of dendritic systems that remained essentially unverified and thus of fundamental interest. Second, the exploration of dendritic molecules with $g \geq g_{max}$ is of practical interest for producing densely packed molecular objects with controllable surface properties and an increased range of tunable spans. Note that while the enhanced tuning range is attained at the price of introducing unavoidable defects at $g \geq g_{max}$, there is little evidence that structural perfection is of practical importance. Apart from the pioneering exploration of the near g_{max} range, this work presents a theoretical framework for quantifying defect statistics on the basis of labelling reactions. It thus introduces a simple technique for the detailed quantitative characterization of dendritic molecules. This technique is especially useful at high g and high molecular masses (MM) where the traditional analytical methods are challenged. It is particularly suitable for the study of g_{max} effects diagnosed via defect quantification at high g.

The synthetic regimes outlined above reflect a distinctive form of steric hindrance. The term steric hindrance typically connotes the prevention of a chemical reaction by a bulky chemical substituent within a molecule[29]. This local effect assumes a novel, global form in dendritic molecules whereby the *overall* density within the molecule reduces the reactivity of certain groups[13]. This effect arises in the vicinity of the so-called de Gennes dense packing limit[30], at $g \simeq g_{max}$, because the bulkier reaction products cannot be accommodated within the available free volume. In turn, the onset of this effect at g_{max} occurs because the mass of an ideal dendron grows exponentially with g while its maximum span increases only linearly[10,12–15]. For $g > g_{max}$ the exponential growth of mass, associated with perfectly regular branching, is impossible. Further growth can only be accommodated by imperfect branching structures leading to sterically induced stoichiometry (SIS)[30], as was first noted by de Gennes and Hervet in 1983 (ref. 13). Since then, the vicinity of g_{max} and the SIS were invoked to rationalize deviations of observed MM from their ideal values[31,32], as well as synthesis failures[33–35]. It was also discussed as a design guideline for controlling the accessibility of the dendritic interior to guest molecules[36,37]. With these exceptions, the accumulated evidence of g_{max} and associated SIS since their prediction in 1983 is scanty and indirect. This state is due to a number of difficulties. On the experimental side, studies confront two problems. First, it is synthetically difficult to approach g_{max} for the often studied dendrimers where estimates suggest $g_{max} \approx 10$ (refs 13,38). Second, the observation of g_{max} effects requires quantification of the frequency of branching defects as a function of g over a wide range of g including the vicinity of g_{max}. This is experimentally challenging because the performance of standard characterization techniques, such as nuclear magnetic resonance (NMR)[39–41], mass spectrometry (MS)[39] and gel permeation chromatography (GPC)[42,43], attain their limits at high g and high MM. While scattering techniques provide information about the dimensions of the dendritic molecules and their density profiles they are not sensitive to branching defects[44,45]. On the theory side, computer simulations probed the onset of dense packing in perfect dendritic molecules by monitoring properties such as bond strain and equilibration rates[38,46,47]. However, these studies do not yield direct information on the occurrence and frequency of structural defects because of their focus on ideally branched structures.

In the following, we report a first direct experimental evidence for the existence of two synthetic regimes due to g_{max} effects and SIS in DP. In particular, we focus on the onset of SIS. Attaining this end required two new inputs: a homologous series of DP with an upper g close to g_{max}, and a theoretical method of analysing the defect labelling data to quantify the defect statistics.

Results

The two new inputs. The first input was enabled by the divergent synthesis of $g = 6$ DP thus producing an extended homologous series of DP with $g = 1...6$, denoted as PGg (Methods). We investigated two homologous series differing in the polymerization degree of the backbone, N: long DP of $N \approx 1{,}000$ ($_{1,000}$PGg) and short DP with $N \approx 45$ ($_{45}$PGg). The $_{1,000}$PG1...$_{1,000}$PG5 series was reported already[48], while the $_{1,000}$PG6 and the $_{45}$PG1...$_{45}$PG6 series are new (Methods). As we shall discuss, the differences between the two have a key role in identifying the g_{max} effects and the onset of SIS. The second, theoretical input is the result of an analysis yielding a recursive equation specifying the average number of junctions and termini from measured quantities.

With these two inputs at hand, the exploration of g_{max} effects in this system is facilitated by three features (a) g_{max} in long DP occurs at lower g range as compared with dendrimers[10,49]. Current estimates for the particular DP studied suggest $6.1 \lesssim g_{max} \lesssim 7.1$ (ref. 50) and thus at the boundary of the $g = 1...6$ homologous series. (b) The DP as synthesized exhibits a single type of defect with no side reactions. In particular, the defect is associated with the occurrence of non-reacted primary amine groups. (c) The number of defects can be quantified via the ultraviolet (UV) absorbance or fluorescence of a label specifically binding to these defects. In this study, the label used is the Sanger reagent[51,52]. In turn, these last two features enable the theoretical analysis of the labelling data of the homologous series of DP in order to quantify the number of defects for different g. As we shall discuss, the number of defects increases significantly for $_{1,000}$PG6 thus suggesting the onset of SIS in the vicinity of g_{max}. Importantly, the effects are evident only in the long $_{1,000}$PGg but not in the short $_{45}$PGg. This supports the SIS interpretation as defect accumulation due to imperfect reaction conversion should affect all DP irrespective of N. In contrast, SIS effects in the g range explored are envisioned only in long, locally cylindrical DP because of their lower g_{max}. They are not expected in the $_{45}$PGg

series because of their higher g_{max} arising since short DP adopts a dendrimer-like, near spherical, shape traceable to backbone end effects.

Synthesis. The divergent synthesis of a dendron proceeds from a f-functional root attached to a point-like core, to a linear polymer chain or to a surface (Fig. 2 and Supplementary Fig. S1). The roots are reacted with X-functional dendronization units (D units), having one reactive functionality and $X-1$ blocked, non-reactive, functional groups. In the next step, the blocked groups of the D units bound to the root are activated and their deblocked groups reacted with newly added D units. A g generation dendron is generated by g iterations of the deblocking reaction sequence. The generation g of the dendron thus specifies the maximal number of branching sites, junctions, along a strand joining the root to a terminal group. In the following, we focus on D units having the overall structure of a dendron junction or, equivalently, a $g=1$ dendron. In other words X is the functionality of the D unit, as well as the number of 'arms' emanating from a junction. In an ideal, structurally perfect g generation dendron each terminal junction bears $X-1$ blocked functionalities and every interior junction involves X bonds between chemically linked D units. Stated differently, the ideal structure contains no free functionalities that is, all functionalities are either blocked or covalently bound to another D unit. In a non-ideal dendron, some of the unblocked functionalities are not reacted and remain free and active (Figs 1 and 2). Additionally, some may undergo side reactions rendering them inactive.

An iterative relationship between the numbers of junctions and of the free or blocked ends. As the theoretical analysis is applicable to dendrimers as well as DP of different chemistries, we formulate it in general terms. Our theory considerations concern 'elementary dendritic motifs': a dendrimer, a repeat unit of a DP comprising of a root with the attached dendrons and the corresponding unit in a dendronized surface. We focus on the simplest case where there are no side reactions and the defects consist of free non-reacted functional groups, 'free ends'. In this case, the structure of generation g dendritic motif is specified by the number of junctions n_g, together with the number of blocked and free ends denoted respectively by k_g^{free} and $k_g^{blocked}$. The total number of ends, free or blocked, in generation g dendritic motif is $k_g^{total}=k_g^{free}+k_g^{blocked}$. In turn, $k_g^{total}=f+(X-2)n_g$ as the functionality of the root is f and each additional junction eliminates one functionality while contributing $X-1$ additional ones. The number of additional junctions generated with the gth synthesis step is denoted by $\Delta n_g \equiv n_g - n_{g-1}$. In a generation g dendritic motif there are n_{g-1} 'non terminal', inner junctions. All Δn_g 'new' junctions are terminal junctions comprising of attached D units each with $(X-1)$ blocked functionalities. Accordingly, the number of blocked terminal functionalities in a dendritic motif of generation g is $k_g^{blocked}=(X-1)\Delta n_g$. Combining $k_g^{blocked}=(X-1)(n_g-n_{g-1})$ with the earlier relationships yields the key recursive equation

$$n_g=(X-1)n_{g-1}+f-k_g^{free} \qquad (1)$$

relating n_g, n_{g-1} and k_g^{free} in a dendritic motif of a given X and f (Fig. 3). It applies to the values characterizing individual dendritic motifs, as well as to ensemble averages denoted by $\langle..\rangle$. Our key result is based on the utilization of Equation (1) to relate $\langle n_g\rangle$, $\langle n_{g-1}\rangle$ and $\langle k_g^{free}\rangle$ of a homologous series of $g=1...\hat{g}$. In this case, it is possible to iteratively solve equation (1) and to obtain $\langle n_1\rangle,...,\langle n_{\hat{g}}\rangle$ from labelling data providing partial information on $\langle k_1^{free}\rangle,...,\langle k_{\hat{g}}^{free}\rangle$, together with the initial values $\langle n_0\rangle=\langle k_0^{free}\rangle=0$. Importantly, the complete set of $\langle n_g\rangle$ thus obtained fully specifies the corresponding $\langle \Delta n_g\rangle$, $\langle k_g^{free}\rangle$ and $\langle k_g^{labelled}\rangle$.

Theoretical analysis of a labelling experiment. To obtain $\langle n_g\rangle$ for the homologous series, we utilize labelling experiments where we measure two concentrations. The first is the molar concentration of labels bound to dendritic molecules of each generation, $c_g^{labelled}$. For the case of efficient labelling reagent considered, we assume that all free ends are labelled and the number of labelled ends per dendritic motif is $k_g^{labelled}=k_g^{free}$. We note that this assumption is tenable only for $g\lesssim g_{max}$. For $g>g_{max}$

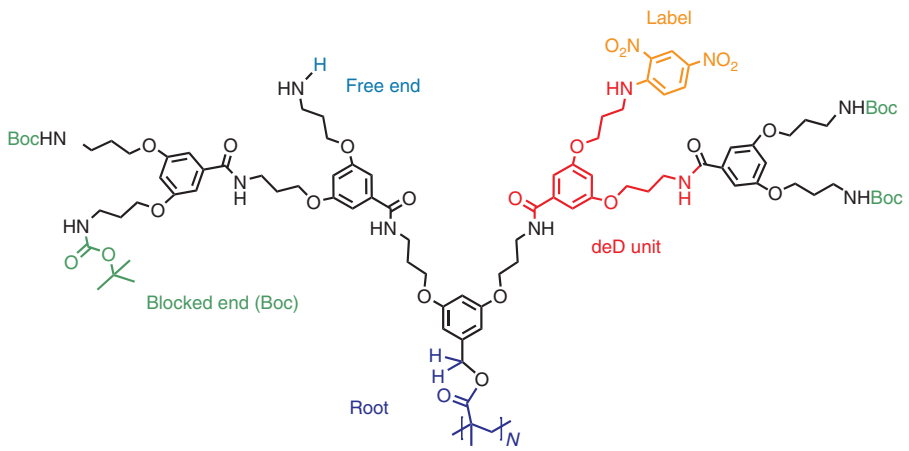

Figure 1 | Structural motifs of our dendrons. The chemical structure of the $g=3$, $X=3$, $f=1$ repeat unit of $_N$PG3 depicting the structural motifs invoked in the analysis: a root, blocked ends, a free end, a bound label and the deD unit forming an internal junction. This structure contains two defects, associated with strands containing $g=2$ junctions. It contains both a labelled and a free end, although in our discussion of the $g\leq g_{max}$ range we assume that all ends are quantitatively labelled and the two motifs may coexist only for $g>g_{max}$. The structures utilized for calculating the characteristic MM of the dendron are coloured $M_O=71.1\,g\,mol^{-1}$ (blue), $M_{deD}=249.29\,g\,mol^{-1}$ (red), $\Delta M_{blocked}=101.12\,g\,mol^{-1}$ (green) and $\Delta M_{labelled}=167.1\,g\,mol^{-1}$ (orange). Note that the root M_O incorporates non-contiguous contributions so as to allow specifying the MM of the $g=1$ junction by a single M_{deD}. This definition differs from the customary convention.

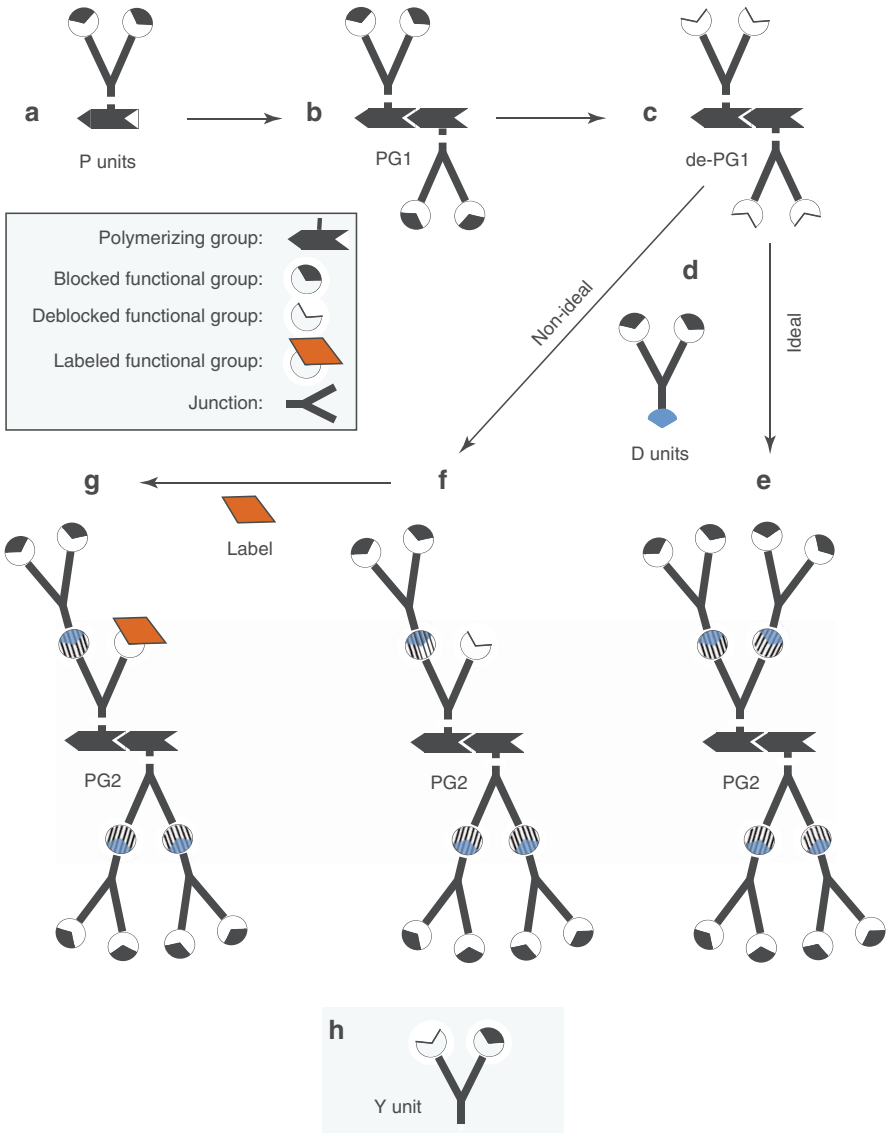

Figure 2 | Schematic view of the synthesis and labelling of DP. P units carrying each two blocked functionalities (**a**) are polymerized to form PG1. As P units are purified, the PG1 is structurally perfect. Conceptually it is useful to consider a polymer backbone with *f*-functional blocked repeat units that is then deblocked and reacted to form a PG1. (**b**) The resulting polymer is deblocked (**c**) and reacted with blocked D units (**d**) to yield PG2. In the ideal case (**e**) all deblocked functionalities are reacted. In reality, certain deblocked functionalities do not react and give rise to free ends (**f**). The amount of free ends is quantified by the absorbance of a labelling agent selectively binding them (**g**). Since the number of terminal groups in a high *g* ideal DP is comparable to the number of inner D units, the typical MM of a branching unit corresponds to a Y unit (**h**).

the free ends at the dendritic interior may be inaccessible to the labels thus leading to $k_g^{\text{labelled}} < k_g^{\text{free}}$. The onset of this effect depends on the size distribution of dendron voids, the size of the label and its interactions. The second measured quantity is the mass concentration of dendritic molecules w/V as specified by the weight of the dry labelled sample, w, and the solvent volume, V. In the following we convert the mass concentration to the molar concentration $c_g^Y = w/VM_Y$ where M_Y is a typical MM of a junction. M_Y accounts for the contributions of both terminal junctions, bearing the two blocking groups, and internal junctions with no blocked groups (Fig. 2): $M_Y = M_{\text{deD}} + (X-2)\Delta M_{\text{blocked}}$ where M_{deD} is the MM of a chemically bound D unit within the 'interior' of the dendron and $\Delta M_{\text{blocked}}$ is the increment of MM of a blocking group bound to a deblocked D unit (Fig. 1). c_g^{labelled} and c_g^Y are both proportional to c_g, the molar concentration of labelled dendritic motifs of generation g: $c_g^{\text{labelled}} = c_g \langle k_g^{\text{labelled}} \rangle$ and $c_g^Y = c_g \langle M_g^{\text{labelled-den}} \rangle / M_Y$ where $\langle M_g^{\text{labelled-den}} \rangle$ is the initially unknown average MM of a labelled dendritic motif of generation g. Their ratio,

$$U_g \equiv \frac{c_g^{\text{labelled}}}{c_g^Y} = \frac{M_Y \langle k_g^{\text{labelled}} \rangle}{\langle M_g^{\text{labelled-den}} \rangle}, \qquad (2)$$

is thus independent of c_g. U_g is a rough estimate of $\langle k_g^{\text{labelled}} \rangle / \langle n_g \rangle$ and it relates $\langle k_g^{\text{labelled}} \rangle$ to the yet to be specified $\langle M_g^{\text{labelled-den}} \rangle$. In turn, $\langle M_g^{\text{labelled-den}} \rangle / M_Y$ is a linear function of $\langle n_g \rangle$ and $\langle n_{g-1} \rangle$ with known coefficients A^{labelled}, B^{labelled}

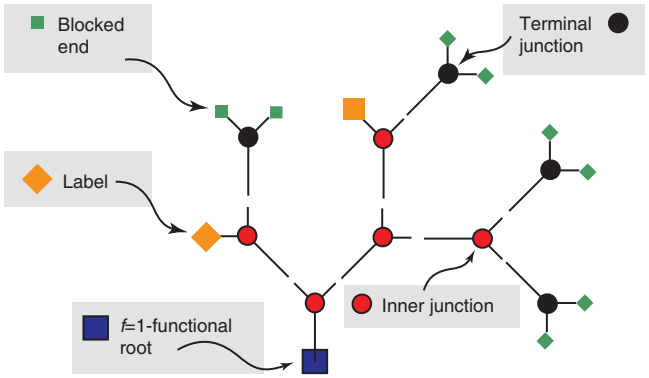

Figure 3 | Recursive relationships. A schematic view of a possible $g=4$, $X=3$, $f=1$ DP dendron depicting $k_4^{\text{labelled}}=2$ labelled ends, $k_4^{\text{blocked}}=8$ blocked ends, $\Delta n_4=4$ terminal junctions and $n_3=5$ inner junctions. When $k_g^{\text{free}}=k_g^{\text{labelled}}$ these quantities obey the following general relationships: $n_4=n_3+\Delta n_4$, $k_4^{\text{blocked}}=(X-1)\Delta n_4$, $k_4^{\text{total}}=f+(X-2)n_4$ and $n_4=(X-1)n_3+f-k_4^{\text{free}}$.

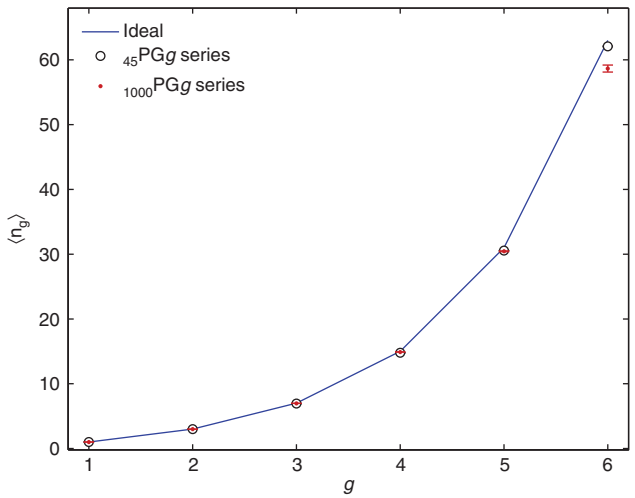

Figure 4 | Junctions per dendron for the members of the homologous series. The number of junctions n_g versus the generation g for both long $_{1,000}$PGg and short $_{45}$PGg series as obtained from the labelling absorbance data upon using equation (3). In the g range studied, the $_{45}$PGg points are indistinguishable from the ideal values given by equation (4). In contrast, the n_g values of the $_{1,000}$PG6 sample deviate from the ideal values. With the exception of $_{1,000}$PG6 the error bars (s.d., Methods) are smaller than the symbols.

and C^{labelled} (Methods and Fig. 1). This, together with equations (1) and (2) yields an iterative equation for $\langle n_g\rangle$, $g=1\ldots\hat{g}$

$$\langle n_g\rangle=\frac{[(X-1)-U_gB^{\text{labelled}}]\langle n_{g-1}\rangle+f-U_gC^{\text{labelled}}}{1+U_gA^{\text{labelled}}} \qquad (3)$$

with the boundary condition $\langle n_0\rangle=0$, as specified by $U_1,\ldots,U_{\hat{g}}$, the three coefficients determined by the chemical structure, as well as f and X (Methods, Fig. 1). For the particular DP investigated in this study, $f=1$ and $X=3$, hence $A^{\text{labelled}}\approx 0.8117$, $B^{\text{labelled}}\approx 0.3766$, and $C^{\text{labelled}}\approx 0.6798$ (Methods). Furthermore PG1 was obtained by polymerization of appropriate P units with $f=1$-functionality bound to a blocked D unit (Fig. 2). Consequently, PG1 can be considered structurally perfect, corresponding to $U_1=0$. Under these circumstances, the first two solutions of equation (3) are accordingly $\langle n_1\rangle=1$ and

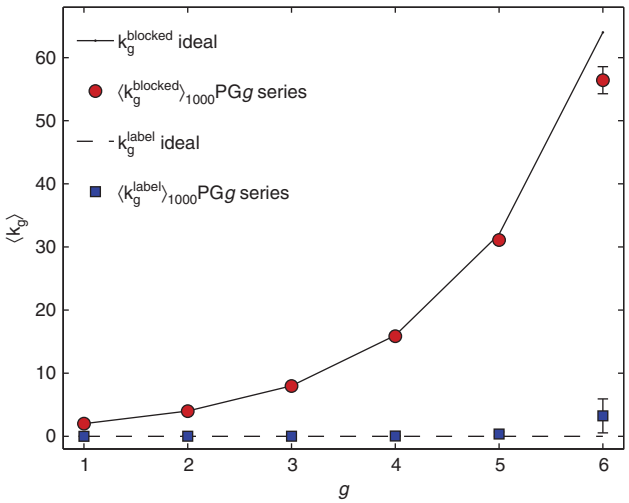

Figure 5 | Blocked and labelled ends per dendron. The number of blocked and labelled ends, k_g^{blocked} and k_g^{labelled} versus the generation g for long $_{1,000}$PGg as compared with the ideal values $k_g^{\text{blocked-ideal}}=f(X-1)^g$ and $k_g^{\text{labelled-ideal}}=0$ (depicted by lines). The $_{1,000}$PG6 points deviate significantly from the ideal curves. In the $1\le g\le 6$ range, the $_{45}$PGg values are indistinguishable from the ideal values and the corresponding points are not displayed. With the exception of $_{1,000}$PG6 the error bars (s.d.) are smaller than the symbols.

$\langle n_2\rangle=[3-U_2(B^{\text{labelled}}+C^{\text{labelled}})]/(1+U_2A^{\text{labelled}})$. Higher g terms are obtained iteratively along the same lines.

Analysis of the labelling measurements. The results of the above analysis of the DP homologous series labelling data are depicted in plots of $\langle n_g\rangle$, $\langle k_g^{\text{blocked}}\rangle$ and $\langle k_g^{\text{labelled}}\rangle$ versus g for both the $_{1,000}$PGg and $_{45}$PGg series (Figs 4 and 5). The $_{45}$PG1...$_{45}$PG6 and $_{1,000}$PG1...$_{1,000}$PG5 are found to exhibit the behaviour of an ideal DP,

$$n_g^{\text{ideal}}=f\frac{(X-1)^g-1}{X-2} \qquad (4)$$

equivalent to equation (3) when $U_g=0$ for all g. In particular, $\langle k_g^{\text{blocked}}\rangle/2$ is indistinguishable from the number of terminal junctions in an ideal structure, $k_g^{\text{blocked-ideal}}=f(X-1)^g$, and there are essentially no free ends, $\langle k_g^{\text{labelled}}\rangle\simeq 0$. In contrast, the $_{1,000}$PG6 results deviate from this trend: $\langle n_6\rangle<n_6^{\text{ideal}}$, $\langle k_6^{\text{blocked}}\rangle<k_6^{\text{blocked-ideal}}$ and $\langle k_6^{\text{labelled}}\rangle\simeq 3.2>0$ (Table 1). The onset of the deviations actually occurs at $_{1,000}$PG5 as can be seen from the $\langle k_g^{\text{labelled}}\rangle/\langle k_g^{\text{blocked}}\rangle$ versus g plot (Fig. 6) that amplifies small deviations that are hard to discern in the $\langle k_g^{\text{labelled}}\rangle$ versus g plot. The upturn in the number of defects occurs below the estimated $g_{\max}$ of this system, $6.1<g_{\max}<7.1$ (ref. 50). However, the onset of packing effects is expected below $g_{\max}$ because the densification of the system slows down transport with corresponding effect on the labelling kinetics. Importantly, the observed deviations occur only for the locally cylindrical $_{1,000}$PGg series. There are no comparable effects for the $_{45}$PGg homologous series, which exhibit ideal DP behaviour as specified by equation (4). This is an important observation supporting the interpretation of the data in terms of $g_{\max}$-related SIS effects. Two arguments are involved. The first concerns the N dependence of $g_{\max}$ and the onset of SIS effects. For long locally cylindrical DP, the current estimate of $g_{\max}$ of this chemistry vary in the $6.1<g_{\max}<7.1$ range[50] and are thus consistent with onset of SIS

Table 1 | Defect characteristics deduced from labelling data of two homologous series.

$_N$PGg	$\langle n_g \rangle$	$\langle k_g^{blocked} \rangle$	$\langle k_g^{labelled} \rangle$
$N \approx 45$ series			
$_{45}$PG2	2.99	3.98	0.01
$_{45}$PG3	6.97	7.95	0.02
$_{45}$PG4	14.89	15.85	0.04
$_{45}$PG5	30.77	31.76	0.01
$_{45}$PG6	62.51	63.49	0.03
$N \approx 1{,}000$ series			
$_{1,000}$PG2	2.99	3.99	0.01
$_{1,000}$PG3	6.97	7.96	0.02
$_{1,000}$PG4	14.90	15.86	0.04
$_{1,000}$PG5	30.44	31.08	0.36
$_{1,000}$PG6	58.65	56.42	3.23

The number of junction units $\langle n_g \rangle$, blocked ends $\langle k_g^{blocked} \rangle$, and labelled ends $\langle k_g^{labelled} \rangle$ for the $_{45}$PGg and $_{1,000}$PGg series. The error bars are specified in the figures with detailed information in the Methods section (Table 2 provides in addition the underlying raw experimental data).

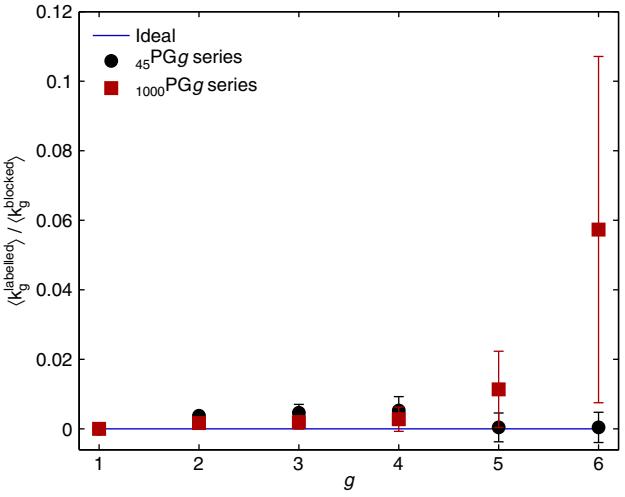

Figure 6 | Onset of branching defects. The ratio $k_g^{labelled}/k_g^{blocked}$ amplifies the deviations from ideal behaviour at the price of larger error bars (s.d.). For short $_{45}$PGg, the ratio $k_g^{labelled}/k_g^{blocked} \simeq 0$ as expected for an ideal DP and ideal dendrimer. In contrast long DPs deviate from ideal at $_{1,000}$PG6 with an onset at $_{1,000}$PG5.

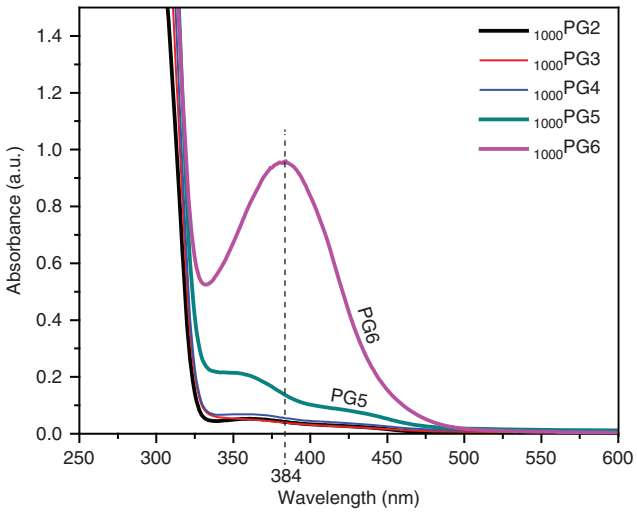

Figure 7 | Experimental labelling data. Plots of the ultraviolet absorbance (A) versus wave length for $_{1,000}$PG2...$_{1,000}$PG6. U_g is calculated from A at $\lambda = 384$ nm (dashed line), the location of the local maximum of the PG6 curve. a.u., arbitrary unit.

at $g \simeq 6$. In contrast, short DP at high g exhibit dendrimer-like configurations because of backbone end effects. This suggests higher g_{max} closer to $12.7 < g_{max} < 14.1$ estimated for dendrimers of similar chemistry[50]. Accordingly, g_{max} effects are not expected for $_{45}$PG1...$_{45}$PG6. The second argument concerns the merits of an alternative explanation of the defect statistics in terms of imperfect conversion of the dendronization reactions. When excluding g_{max}-dependent SIS effects, this second mechanism is expected to affect both $_{45}$PGg and $_{1,000}$PGg homologous series. The absence of such trend supports the interpretation in terms of SIS effects.

Discussion

Utilizing labelling technique we obtained evidence for the onset of SIS g_{max} effects in long DP of $g = 6 \lesssim g_{max}$ close to $6.1 < g_{max} < 7.1$. This result is the first systematic confirmation of packing effects on the synthesis of dendritic molecules since their prediction in 1983. The attainment of $g \approx g_{max}$ is also a first step towards the methodical exploration of $g > g_{max}$ dendritic molecules of interest as dense molecular objects with tunable size. Finally, the labelling technique, together with the theoretical framework reported, is a promising characterization technique for a significant family of dendritic molecules. As we shall discuss, it balances advantages, due to light instrumental and computational requirements, with shortcomings regarding its range of applicability. The labelling technique is applicable when four conditions are satisfied: (i) A homologous series of dendritic molecules $g = 1...\hat{g}$ is available. This is typically the case when utilizing divergent synthesis. (ii) The dominant defects are non-reacted, deblocked terminal groups. This is often the case for divergent synthesis using $g = 1$ dendrons as D units. This condition is realized, for example, in Denkewalters dendritic peptides[17], Newkomes arborols[18] and in Simaneks triazin-based dendrimers[53]. (iii) The defects can be efficiently interrogated by a labelling reagent. There is no universal label and the choice of the reagent should be customized to the synthetic chemistry used. When NH_2 groups are involved one may use the Sanger reagent[51,52] or Dansyl[54–56]. The Sanger reagent is less prone to aggregation and its smaller size is advantageous at high g. (iv) The labelling method can quantify all free ends for $1 \leq g \lesssim g_{max}$, that is, $\langle k_g^{labelled} \rangle = \langle k_g^{free} \rangle$. For $g > g_{max}$, it provides an efficient probe of exterior, accessible, free ends. However, the labels may encounter steric hindrance when binding defects situated within the dense dendritic interior that is,, $\langle k_g^{labelled} \rangle < \langle k_g^{free} \rangle$. When these four requirements are met, the labelling method yields $\langle n_g \rangle$, $\langle \Delta n_g \rangle$, $\langle k_g^{free} \rangle$ and $\langle k_g^{blocked} \rangle$ for $g = 1...\hat{g}$ thus providing a complete characterization of the average structure. In particular, it specifies the average MM of the dendritic motif via equation (5) or its counterpart for the non-labelled moiety. MS when applicable, is free of these limitations[31,39]. However, it requires a dedicated facility and significant computational effort to deconvolute the spectra. In marked contrast, the labelling approach based on the Sanger method requires a ultraviolet spectrophotometer and minimal computational effort. With regard to MS and NMR, one should also note difficulties in characterizing high g dendritic molecules in general and DP in particular. These difficulties are even more pronounced for GPC.

The interest in dendritic molecules is motivated in part by the vision of single-molecule colloidal particles of well-defined

chemical structure. This direction is illustrated by $_{17,600}$PG5, a single-molecule comparable in length and width to the potyvirus family and common cytoskeleton fibrils[48,57]. If one adheres to this point of view, it is important to establish g_{max} because it signals the onset of SIS thus setting the upper boundary of synthetically attainable ideal dendritic molecules. However, the 'post g_{max}' regime may afford opportunities in spite of the unavoidable structural defects. Along the lines of the de Gennes–Hervet argument one may hypothesize that the structure of $g > g_{max}$ dendritic molecules is controlled by packing constraints resulting in dense molecules with well-defined dimensions. The investigation of this hypothesis again requires knowledge of g_{max}, as well as efficient defect quantification methods for the g_{max} range. Note that defects affect properties of dendritic molecules that depend on the number of end-groups, such as solubility. These observations confront a current lack of systematic observations of g_{max} effects traceable to synthetic and characterization difficulties facing the exploration of the g_{max} range. In this context, our work pioneers the synthesis of near g_{max} DP and the quantitative exploration of the branching defects associated with SIS. It thus initiates the systematic investigation of the $g \gtrsim g_{max}$ regime.

Methods

Synthesis of deblocked *de*-$_{1,000}$PG5. Some of the starting material, denoted by $_{1,000}$PG5, may have undergone charge-assisted, shear-induced main chain cleavage[58], thus resulting in product of lower *N*. To a slowly- stirred, freeze-dried powder of $_{1,000}$PG5 (0.20 g, 0.018 mmol repeat units) in a round bottom flask was dropwise added trifluoroacetic acid (TFA) (25 ml) and methanol (1 ml) at 0 °C. The reaction mixture soon turned homogeneous and was stirred at room temperature for 1 h. Then methanol (20 ml) was added and the mixture was evaporated in vacuo. This methanol addition and evaporation procedure was repeated twice, thereafter the residue was dissolved in water (15 ml) and carefully lyophilized to yield *de*-$_{1,000}$PG5 as a powdery white solid (0.21 g, 100%). 1H NMR (500 MHz, DMF-d7): $\delta = 0.90$ (br, 18H, CH_3), 1.33 (br, 45H, CH_3), 2.01–2.19 (br, 326H, CH_2), 3.20–3.49 (br, 252H, CH_2NH), 4.12 (br, 252H, CH_2O), 6.42 (br, 75H, Ph), 7.08 (br, 142H, Ph), 8.41 (br, 30H, Ph, NH). Note: It is essential to avoid exposure of the *de*-$_{1,000}$PG5 to shear forces because the chains can suffer a charge-assisted, shear-induced main chain cleavage[58].

Synthesis of blocked $_{1,000}$PG6. To a dimethylformamide (DMF) solution (250 ml) of *de*-$_{1,000}$PG5 (200 mg, 0.0174 mmol repeat unit) at −5 °C was added triethylamine (88 mg, 0.87 mmol) and N,N-dimethylaminopyridine (DMAP) (30 mg, 0.25 mmol). A solution of the D unit, the active ester dendron DG1 (3.15 g, 5.57 mmol) was added in six portions over 20 days. During the addition of each portion, the reaction mixture was cooled to −5 °C, then slowly warmed to room temperature and stirred for 3–4 days. After the addition of all the active ester dendron DG1, the reaction mixture was left stirring for another 10 days, then concentrated in vacuo. The residue was dissolved in 20 ml of dichloromethane (DCM) followed by column chromatography purification (eluent: DCM, Rf = 0.1). This produced a beige gel, which was freeze-dried from 1,4-dioxane (40 ml) to yield $_{1,000}$PG6 as a powdery, white solid (78 mg, 20%). 1H NMR (500 MHz, DMF-d7): $\delta = 0.91$ (br, 45H, CH_3),1.36 (br, 576H, CH_3), 1.89–2.02 (br, 273H, CH_2), 3.04 (br, 134H, CH_2), 3.18 (br, 153H, CH_2), 3.62 (br, 99H, CH_2), 4.08 (br, 252H, CH_2), 6.19 (br, 66H, CH), 6.58 (br, 79H, CH), 7.05 (br, 144H, CH), 8.16 (br, 45H, NH). Calcd for $(C_{1143}H_{1654}N_{126}O_{318})_N$: C, 61.71; H, 7.49; N, 7.93. Found: C, 61.19; H, 7.20; N, 7.52.

Synthesis of $_{45}$PG1…$_{45}$PG6. $_{45}$PG1 was synthesized by a reversible addition-fragmentation chain transfer (RAFT) protocol according to the reported procedure[59]. Divergent synthesis of $_{45}$PG2...$_{45}$PG6: to a solution of deprotected polymer precursor *de*-$_{45}$PG(*g*-1) in DMF was added 4-dimethylaminopyridine (DMAP, cat.) and triethylamine (TEA, 2 eq. per amine) at −5 °C. Dendron active ester DG1 (5 eq. per amine) was added in three portions over a total predetermined time (4–15 days). Each portion was added at −5 °C, followed by a stirring at room temperature for 1–5 days. After the addition of the last portion and stirring, the reaction mixture was concentrated in vacuo. The residue was dissolved in DCM and purified by column chromatography (silica gel, DCM eluent) to give a beige gel, which was lyophilized from 1,4-dioxane to yield the product $_{45}$PG*g* as a white powder (71–88%). Normalized GPC elution curves of $_{45}$PG1...$_{45}$PG6 are provided in Supplementary Fig. S2.

Labelling the DP. To a well-stirred solution of blocked DP (5.0 mg) in 1,1,2,2-tetrachloroethane (0.3 ml) was added 0.1 M $NaHCO_3$ solution (0.043 ml), and a solution of Sanger reagent (0.4 mg, 0.3 eq. per Boc) was added in 1,1,2,2-tetrachloroethane (0.04 ml). The reaction mixture was stirred at 65 °C for 3 h, and then cooled to room temperature. 1,1,2,2-tetrachloroethane (2 ml), water (2 ml) and citric acid (1 mg) were added to the mixture. The organic layer was separated, washed by water (1 ml) and brine (1 ml), and concentrated in vacuo. The residue was dissolved in tetrahydrofuran (1 ml) and precipitated into methanol/water (4:1). This procedure was repeated four times to yield the labelled polymer in the form of a yellow solid (3.5 mg, 70%).

Ultraviolet absorbance measurements. Measurements (Fig. 7) were performed on a Perkin Elmer Lambda 20 and a Jasco V-670 ultraviolet–vis spectrometer using 1 mm or 2 mm quartz cells, respectively. The labelled $_{1,000}$PG6 was dissolved homogeneously in 1,1,2,2-tetrachloroethylene. The extinction coefficient $\varepsilon = 1.64 \times 10^4\ l\,mol^{-1}\,cm^{-1}$ (ref. 52) was assumed for 2,4-dinitroaniline moieties. Their concentration was calculated using the Lambert–Beer law ($c^{labelled} = A/\varepsilon l$), in which $l = 0.1$ cm ($_{1,000}$PG*g*) or $l = 0.2$ cm ($_{45}$PG*g*) denotes the interior width of the quartz cell and A the absorbance at wave length $\lambda = 384$ nm (Fig. 7).

Derivation of equation (3). The dimensionless coefficients $A^{labelled}$, $B^{labelled}$ and $C^{labelled}$ occurring in

$$\frac{\langle M_g^{labelled\text{-}den}\rangle}{M_Y} = A^{labelled}\langle n_g\rangle + B^{labelled}\langle n_{g-1}\rangle + C^{labelled} \qquad (5)$$

Table 2 | Summary of measured raw data and derived defect characteristics for the $_{45}$PG*g* and $_{1,000}$PG*g* series.

	Measured				Derived						
$_N$PG*g*	*w* (mg)	w_s (g)	*V* (ml)	*A*	c_g^{labels} (mmol l^{-1})	U_g	$\langle n_g\rangle$	$\langle k_g^{blocked}\rangle$	$\langle k_g^{labelled}\rangle$	M_g^{ideal} (g mol^{-1})	$\langle M_g^{labelled-den}\rangle$ (g mol^{-1})
N ≈ 45 series											
$_{45}$PG2	8.48	1.5881	0.9944	0.1725	0.0526	0.00216	2.99	3.98	0.01	1,223.5	1,221
$_{45}$PG3	8.32	1.5804	0.9919	0.1925	0.0587	0.00245	6.97	7.95	0.02	2,625.1	2,615
$_{45}$PG4	8.38	1.5962	0.9995	0.2132	0.0650	0.00272	14.89	15.85	0.04	5,428.5	5,393
$_{45}$PG5	4.24	2.3987	1.5020	0.0112	0.0034	0.00042	30.77	31.76	0.01	11,035.1	10,955
$_{45}$PG6	2.52	1.2009	0.7529	0.0132	0.0040	0.00042	62.51	63.49	0.03	22,248.4	22,079
N ≈ 1,000 series											
$_{1,000}$PG2	5.7	1.5342	0.9606	0.0527	0.0322	0.00190	2.99	3.99	0.01	1,223.5	1,222
$_{1,000}$PG3	5.3	1.5060	0.9430	0.0531	0.0324	0.00202	6.97	7.96	0.02	2,625.1	2,616
$_{1,000}$PG4	3.5	1.0827	0.6780	0.0692	0.0422	0.00286	14.90	15.86	0.04	5,428.5	5,396
$_{1,000}$PG5	4.4	7.9442	4.9745	0.0477	0.0291	0.01152	30.44	31.08	0.36	11,035.1	10,863
$_{1,000}$PG6	4.3	3.4285	2.1470	0.5067	0.3090	0.05410	58.65	56.42	3.23	22,248.4	20,938

w denotes the mass of the labelled polymer, w_s the mass of the solution. Volume *V* of the polymer solution is calculated from the measured masses $w_s = \rho V$ with $\rho = 1.597$ g cm^{-3} assuming the density of the dilute polymer solution is the same as that of the pure solvent 1,1,2,2-tetrachloroethane. The molar concentration of labels c_g^{labels} is calculated from the measured ultraviolet absorbance *A* (Methods). $U_g = c_g^{labels} M_Y V/w$ with $M_Y = 350.415$ g mol^{-1}. The reference mass of an ideal PG*g* is $M_g^{ideal} = 2^g \times M_Y - 178.191$ g mol^{-1}. Error bars calculated using equation 9 and equation 10 are provided in the figs.

are determined uniquely by the chemical structure

$$A^{\text{labelled}} = [M_{\text{deD}} + (X-1)\Delta M_{\text{blocked}} - \Delta M_{\text{labelled}}]/M_Y,$$

$$B^{\text{labelled}} = (X-1)(\Delta M_{\text{labelled}} - \Delta M_{\text{blocked}})/M_Y,$$

$$C^{\text{labelled}} = (M_0 + f\Delta M_{\text{labelled}})/M_Y \quad (6)$$

All masses entering equation 6 had been introduced in Fig. 1. Equation (5) with equation (6) follows from the mass accounting relationship $M_g^{\text{labelled-den}} = M_0 + n_g M_{\text{deD}} + k_g^{\text{blocked}}\Delta M_{\text{blocked}} + k_g^{\text{labelled}}\Delta M_{\text{labelled}}$ upon substituting $k_g^{\text{blocked}} = (X-1)(n_g - n_{g-1})$ and allowing for $k_g^{\text{total}} = k_g^{\text{blocked}} + k_g^{\text{labelled}} = f + (X-2)n_g$. Insertion of $\langle k_g^{\text{free}} \rangle = U_g[A^{\text{labelled}}\langle n_g \rangle + B^{\text{labelled}}\langle n_{g-1} \rangle + C^{\text{labelled}}]$ into equation (1) leads to equation (3).

Error estimates. The masses of the labelled polymer samples, w, and masses of the solution, w_s, were measured up to a precision of $\delta w = 0.1$ mg and $\delta w_s = 10$ mg, respectively, taking into account both instrumental and evaporation errors. The volumes of the polymer solutions are calculated from the measured masses, $V = w_s/\rho$ with $\rho = (1.597 \pm 0.001)\,\text{g cm}^{-3}$ assuming the density of the dilute polymer solution is identical with that of the pure solvent (Table 2). The molar concentrations of labels $c_g^{\text{labels}} = A/\epsilon l$ had been determined from the ultraviolet adsorbances A that come with a maximal relative error of 2% for the $_{45}$PGg series (measured with Jasco V-670 (ref. 60)), and 4% for the $_{1,000}$PGg series (Perkin Elmer Lambda 20 (refs 48,15)). The error of the denominator follows from $\delta\epsilon \approx 100$ (ref. 52) and $\delta l \approx 1$ micron. The relevant ratios

$$U_g = \frac{M_Y V}{w} c_g^{\text{labels}} = \frac{w_s M_Y}{w\rho}\frac{A}{\epsilon l} \quad (7)$$

furthermore involve our reference mass of a typical branching unit, $M_Y = (350.415 \pm 0.001)\,\text{g mol}^{-1}$. The relative error $\delta U_g/U_g$ thus follows immediately from the reported values in Table 2 and their above-mentioned errors by summing up the relative errors for all quantities on the rhs of equation 7.

The calculation of $\langle n_g \rangle$ via the iterative relationship (equation 3 with $f = 1$ and $X = 3$)

$$\langle n_g \rangle = \frac{(2 - B^{\text{labelled}}U_g)\langle n_{g-1} \rangle + (1 - C^{\text{labelled}}U_g)}{1 + A^{\text{labelled}}U_g} \quad (8)$$

involves the dimensionless constants A^{labelled}, B^{labelled} and C^{labelled}. As the chemical structure of the ideal dendron is known exactly, the relative error of these three coefficients is negligible. $\langle n_1 \rangle = 1$ being error free as discussed within the Results section. The error of $\langle n_g \rangle$ remains to be determined for given value and error of the preceding $\langle n_{g-1} \rangle$ and the calculated $U_g \pm \delta U_g$. Fortunately, the errors δU_g occur in combinations of the form $1 + A^{\text{labelled}}U_g$. Importantly, because $\delta U_g \ll 1$ and because all coefficients A^{labelled}, B^{labelled} and C^{labelled} are of order unity, the relative error $\delta\langle n_g \rangle$ is mainly determined by $(X-1)\delta\langle n_{g-1} \rangle$ alone, and does not grow exponentially. Furthermore, for $g = 4$ or higher, when $\langle n_{g-1} \rangle \gg 1$, the last bracket in the nominator of equation 8 becomes clearly irrelevant.

If we denote the absolute error of $\langle n_g \rangle$ with $\delta\langle n_g \rangle$ its relative error is

$$\frac{\delta\langle n_g \rangle}{\langle n_g \rangle} = \frac{c_1\delta\langle n_{g-1} \rangle + c_2\delta U_g}{c_3(1 + A^{\text{labelled}}U_g)} \quad (9)$$

with coefficients

$$c_1 = (1 + A^{\text{labelled}}U_g)(2 - B^{\text{labelled}}U_g),$$

$$c_2 = A^{\text{labelled}} + C^{\text{labelled}} + (2A^{\text{labelled}} + B^{\text{labelled}})\langle n_{g-1} \rangle,$$

$$c_4 = (1 - C^{\text{labelled}}U_g)(2 - B^{\text{labelled}}U_g)\langle n_{g-1} \rangle \quad (10)$$

For example ($g = 2$):

$$\frac{\delta\langle n_2 \rangle}{\langle n_2 \rangle} = \frac{(3A^{\text{labelled}} + B^{\text{labelled}} + C^{\text{labelled}})\delta U_1}{(1 + A^{\text{labelled}}U_1)(3 - C^{\text{labelled}}U_1 - B^{\text{labelled}}U_1)} \approx \frac{(3A^{\text{labelled}} + B^{\text{labelled}} + C^{\text{labelled}})}{3}\delta U_1 \quad (11)$$

As $\langle n_1 \rangle = 1$, and this yields $\approx 1.2 \times \delta U_1$ for the numerical values of A^{labelled}, B^{labelled} and C^{labelled} that are specified after equation 3.

References

1. Newkome, G. R., Moorefield, C. N. & Vögtle, F. *Dendritic Macromolecules: Concepts, Syntheses, Perspectives* (VCH, 1996).
2. Fréchet, J. M. J. & Tomalia, D. A. eds. *Dendrimers and Other Dendritic Polymers* (Wiley & Sons, 2001).
3. Vögtle, F., Richardt, G. & Werner, N. *Dendrimer Chemistry* (Wiley VCH, 2009).
4. Caminade, A. -M., Turrin, C. -O., Laurent, R., Quali, A. & Delavaux-Nicot, B. *Dendrimers: Towards Catalytic, Material and Biomedical Uses* (Wiley & Sons, 2011).
5. Campagna, S., P., F. & Ceroni, P. eds. *Designing Dendrimers* (Wiley & Sons, 2011).
6. Schlüter, A. D. & Rabe, J. P. Dendronized polymers: Synthesis, characterization, assembly at interfaces, and manipulation. *Angew. Chem. Int. Ed.* **39,** 864–883 (2000).
7. Schlüter, A. D. A covalent chemistry approach to giant macromolecules with cylindrical shape and an engineerable interior and surface. *Top. Curr. Chem.* **245,** 151–191 (2005).
8. Frauenrath, H. Dendronized polymers building a new bridge from molecules to nanoscopic objects. *Prog. Polym. Sci.* **30,** 325–384 (2005).
9. Rosen, B. M., Wilson, C. J., Wilson, D. A., Peterca, M., Imam, M. R. & Percec, V. Dendron-mediated self-assembly, disassembly, and self-organization of complex systems. *Chem. Rev.* **109,** 6275–6540 (2009).
10. Kröger, M., Peleg, O. & Halperin, A. From dendrimers to dendronized polymers and forests: scaling theory and its limitations. *Macromolecules* **43,** 6213–6224 (2010).
11. Benhabbour, S. R., Sheardown, H. & Adronov, A. Protein resistance of PEGfunctionalized dendronized surfaces: effect of PEG molecular weight and dendron generation. *Macromolecules* **41,** 4817–4823 (2008).
12. Tomalia, D. A., Naylor, A. M. & Goddard, III W. A. Starburst dendrimers - molecular-level control of size, shape, surface-chemistry, topology, and flexibility from atoms to macroscopic matter. *Angew. Chem. Int. Ed.* **29,** 138–175 (1990).
13. de Gennes, P. G. & Hervet, H. Statistics of starburst polymers. *J. Phys. Lett.* **44,** L351–L360 (1983).
14. Boris, D. & Rubinstein, M. A self-consistent mean field model of a starburst dendrimer: dense core vs dense shell. *Macromolecules* **29,** 7251–7260 (1996).
15. Guo, Y. *et al.* Tuning polymer thickness: synthesis and scaling theory of homologous series of dendronized polymers. *J. Am. Chem. Soc.* **131,** 11841–11854 (2009).
16. Tomalia, D. A. *et al.* A new class of polymers - starburst-dendritic macromolecules. *Polym. J.* **17,** 117–132 (1985).
17. Denkewalter, R. G., Kolc, J. & Lukasavage, W. J. Macromolecular highly branched homogeneous compound based on lysine units. US Patent no. 4,289,872 (1981).
18. Newkome, G. R., Yao, Z. -Q., Baker, G. R. & Gupta, V. K. Micelles. 1. Cascade molecules - a new approach to micelles. *J. Org. Chem.* **50,** 2003–2004 (1985).
19. Buhleier, E., Wehner, W. & Vögtle, F. Cascade-chain-like and nonskid-chain-like syntheses of molecular cavity topologies. *Synthesis* **2,** 155–158 (1978).
20. Lee, C. C., MacKay, J. A., Fréchet, J. M. J. & Szoka, F. Designing dendrimers for biological applications. *Nat. Biotechnol.* **23,** 1517–1526 (2005).
21. Knapen, J. W. J. *et al.* Homogeneous catalysts based on silane dendrimers functionalized with acrylnickel(II) complexes. *Nature* **372,** 659–663 (1994).
22. Astruc, D. Electron-transfer processes in dendrimers and their implication in biology, catalysis, sensing and nanotechnology. *Nat. Chem.* **4,** 255–267 (2012).
23. Percec, V., Ahn, C. H., Ungar, G., Yeardley, D. J. P., Moller, M. & Sheiko, S. S. Controlling polymer shape through the self-assembly of dendritic side-groups. *Nature* **391,** 161–164 (1998).
24. Astruc, D., Boisselier, E. & Ornelas, C. Dendrimers designed for functions: from physical, photophysical, and supramolecular properties to applications in sensing, catalysis, molecular electronics, photonics, and nanomedicine. *Chem. Rev.* **110,** 1857–1959 (2010).
25. Menjoge, A. R., Kannan, R. M. & Tomalia, D. A. Dendrimer-based drug and imaging conjugates: design considerations for nanomedical applications. *Drug. Discov. Today.* **15,** 171–185 (2010).
26. Tekade, R. K., Kumar, P. V. & Jain, N. K. Dendrimers in oncology: an expanding horizon. *Chem. Rev.* **109,** 49–87 (2009).
27. Rosen, B. M., Wilson, C. J., Wilson, D. A., Peterca, M., Imam, M. R. & Percec, V. Dendron-mediated self-assembly, disassembly, and self-organization of complex systems. *Chem. Rev.* **109,** 6275–6540 (2009).
28. Mintzer, M. A. & Simanek, E. E. Nonviral vectors for gene delivery. *Chem. Rev.* **109,** 259–302 (2009).
29. March, J. *Advanced Organic Chemistry: Reactions, Mechanisms, Structure* 4th edn (J. Wiley, New York, 1992).
30. Tomalia, D. A., Christensen, J. B. & Boas, U. *Dendrimers, Dendrons and Dendritic Polymers: Discovery, Applications, the Future* (Cambridge University Press, 2012).
31. Tomalia, D. A. Dendritic effects: dependency of dendritic nano-periodic property patterns on critical nanoscale design parameters (CNDPs). *New. J. Chem.* **36,** 264–281 (2012).
32. Ornelas, C., Ruiz, J., Belin, C. & Astruc, D. Giant dendritic molecular electrochrome batteries with ferrocenyl and pentamethylferrocenyl termini. *J. Am. Chem. Soc.* **131,** 590–601 (2009).
33. Swanson, D. R., Huang, B. H., Abdelhady, H. G. & Tomalia, D. A. Unique steric and geometry induced stoichiometries observed in the divergent synthesis of poly(ester-acrylate/amine) (PEA) dendrimers. *New J. Chem.* **31,** 1368–1378 (2007).

34. Kawaguchi, T., Walker, K. L., Wilkins, C. L. & Moore, J. S. Double exponential dendrimer growth. *J. Am. Chem. Soc.* **117,** 2159–2165 (1995).
35. Lothian-Tomalia, M. K., Hedstrand, D. M., Tomalia, D. A., Padias, Jr B. & H., K. H. A Contemporary survey of covalent connectivity and complexity. the divergent synthesis of poly(thioether) dendrimers. amplified, genealogically directed synthesis leading to the de gennes dense packed state. *Tetrahedron* **53,** 15495–15513 (1997).
36. Tomalia, D. A. Birth of a new macromolecular architecture: dendrimers as quantized building blocks for nanoscale synthetic organic chemistry. *Aldrichim Acta.* **37,** 39–57 (2004).
37. Jansen, J. F. G. A., de Brabander-van den Berg, E. M. M. & Meijer, E. W. Encapsulation of guest molecules into a dendritic box. *Science* **266,** 1226–1229 (1994).
38. Maiti, P. K., Cagin, T., Wang, G. & Goddard, III W. A. Structure of PAMAM dendrimers: generations 1 through 11. *Macromolecules* **37,** 6236–6254 (2004).
39. Hummelen, J. C., van Dongen, J. L. J. & Meijer, E. W. Electrospray mass spectrometry of poly(propylene imine) dendrimers - the issue of dendritic purity or polydispersity. *Chem. Eur. J.* **3,** 1489–1493 (1997).
40. Wilson, L. R. & Tomalia, D. A. Synthesis and characterization of starburst dendrimers. *Prepr. Am. Chem. Soc. Div. Polym. Chem.* **30,** 115–120 (1989).
41. Smith, P. B., Martin, S. J., Hall, M. J. & Tomalia, D. A. *Applied Polymer Analytics and Characterization* (Hanser, 1987).
42. Hawker, C. J. & Fréchet, J. M. J. Preparation of polymers with controlled molecular architecture - a new convergent approach to dendritic macromolecules. *J. Am. Chem. Soc.* **112,** 7638–7647 (1990).
43. Wooley, K. L., Hawker, C. J. & Fréchet, J. M. J. Hyperbranched macromolecules via a novel double-stage convergent growth approach. *J. Am. Chem. Soc.* **113,** 4252–4261 (1991).
44. Mallamace, F. *et al.* Scaling properties in the internal structure of dendrimer systems. *Physica A* **304,** 235–243 (2002).
45. Ballauff, M. & Likos, C. N. Dendrimers in solution: insight from theory and simulation. *Angew. Chem. Int. Ed.* **43,** 2998–3020 (2004).
46. Chen, Z. Y. & Cui, S. -M. Monte Carlo simulations of star-burst dendrimers. *Macromolecules* **29,** 7943–7952 (1996).
47. Klos, J. S. & Sommer, J. -U. Properties of dendrimers with flexible spacer-chains: a monte carlo study. *Macromolecules* **42,** 4878–4886 (2009).
48. Zhang, B. *et al.* The Largest synthetic structure with molecular precision: towards a molecular object. *Angew. Chem. Int. Ed.* **50,** 737–740 (2011).
49. Zhang, Z. -B., Teng, Y. -H., Freas, W. & Mohanty, D. K. Unimolecular Amphiphilic nanocontainers based on dendronized linear polymers. *Macromol. Rapid Commun.* **27,** 626–630 (2006).
50. Zhang, B., Wepf, R., Kröger, M., Halperin, A. & Schlüter, A. D. Height and width of adsorbed dendronized polymers: electron and atomic force microscopy of homologous series. *Macromolecules* **44,** 6785–6792 (2011).
51. Sanger, F. & Thompson, E. O. P. The amino-acid sequence in the glycyl chain of insulin. 1. The identification of lower peptides from partial hydrolysates. *Biochem. J.* **53,** 353–366 (1953).
52. Shu, L., Gössl, I., Rabe, J. P. & Schlüter, A. D. Quantitative aspects of the dendronization of dendronized linear polystyrenes. *Macromol. Chem. Phys.* **203,** 2540–2550 (2002).
53. Steffensen, M. B. & Simanek, E. E. Synthesis and manipulation of orthogonally protected dendrimers: building blocks for library synthesis. *Angew. Chem. Int. Ed.* **43,** 5187–5180 (2004).
54. Vögtle, F., Gestermann, S., Kauffmann, C., Ceroni, P., Vicinelli, V. & Balzani, V. Coordination of Co2+ ions in the interior of poly(propylene amine) dendrimers containing fluorescent dansyl units in the periphery. *J. Am. Chem. Soc.* **122,** 10398–10404 (2000).
55. Balzani, V. & Vögtle, F. Dendrimers as luminescent hosts for metal cations and organic molecules. *CR Chimie* **6,** 867–872 (2003).
56. Zhang, W., Tichy, S. E., Pérez, L. M., Maria, G. C., Lindahl, P. A. & Simanek, E. E. Evaluation of multivalent dendrimers based on melamine: kinetics of thiol-disulfide exchange depends on the structure of the dendrimer. *J. Am. Chem. Soc.* **125,** 5086–5094 (2003).
57. Fletcher, D. A. & Mullins, D. Cell mechanics and the cytoskeleton. *Nature* **463,** 485–492 (2010).
58. Yu, H., Schlüter, A. D. & Zhang, B. Main-chain scission of a charged fifth-generation dendronized polymer. *Helv. Chim. Acta.* **95,** 2399–2410 (2012).
59. Yu, H., Schlüter, A. D. & Zhang, B. Synthesis of dendronized polymers by a '$n+2$' approach. *Macromolecules* **45,** 8555–8560 (2012).
60. Junker, K., Zandomeneghi, G., Guo, Z., Kissner, R., Ishikawa, T. & Kohlbrecher, J. Mechanistic aspects of the horseradish peroxidase-catalysed polymerisation of aniline in the presence of AOT vesicles as templates. *RSC Adv.* **2,** 6478–6495 (2012).

Acknowledgements

We thank Dr Bernd Bruchmann, BASF and Prof. Dr Renato Zenobi, ETH Zürich for helpful discussions.

Author contributions

A.D.S., A.H. and M.K. designed research. B.Z. and H.Y. performed experiments. M.K. developed model. M.K. and B.Z. analysed data. A.H. wrote the paper.

Additional information

Supplementary Information accompanies this paper at www.nature.com/naturephysics.

Competing Financial Interests: The authors declare no competing financial interests.

Reprints and permission information is available online at http://www.nature.com/reprintsandpermissions/

How to cite this article: Zhang, B. *et al.* Synthetic regimes due to packing constraints in dendritic molecules confirmed by labelling experiments. *Nat. Commun.* 4:1993 doi: 10.1038/ncomms2993 (2013).